nature geoscience
SUPPLEMENTARY INFORMATION
DOI: 10.1038/NGEO2299

Thick and deformed Antarctic sea ice mapped with autonomous underwater vehicles

G. Williams, T. Maksym, J. Wilkinson, C. Kunz, C. Murphy, P. Kimball, H. Singh

Assessment of Ice Type: First Year versus Multiyear Floes

All of the surveyed floes are most likely to be first year (FY) floes based on multiple lines of evidence (Table S1, Fig S1, S2). While in most cases MY ice is distinguished from thinner FY ice by the deep snow cover, thick ice and high freeboard, discrimination is more difficult in our case where the FY ice was also thick and heavily deformed and most floes had a deep snow cover. This evidence includes imagery showing lack of ice in the region at the end of the previous summer, ice morphology, ice properties, and snow cover characteristics. Evidence of each of the above listed characteristics is given for each floe in Table S1 along with an indication of whether each property is suggestive of FY or MY ice.

ENVISAT Synthetic Aperture Radar (SAR) for the Bellingshausen Sea (February 14 and March 26, 2010) and Wilkes Land (March 8, 2012) show open water at the location of each survey site (Fig. S1). Because of the almost complete melt of ice in the summer of 2010 in the Bellingshausen, MY ice is unlikely to have drifted into the survey areas, with the exception of floes 1 and 2, where some MY ice floes from north of the Wilkins ice shelf may have entered the area. However, ice continued to be exported westward from this area over the next several months, reducing the chance of MY ice being in the survey area. For Floe 2, which was at the edge of the MY ice in February/March, the ice thickness of the level pans on this floe was 1.35 m, which is more likely to be from FY ice. In the embayment between Latady Island and Beethoven Peninsula (Floes 3 and 4) the direction of export is westward out of the embayment, so MY ice is unlikely to enter the region after freeze-up. In the Weddell Sea, the survey area is an area of a mixture of drifting MY and FY pack. The surveyed floes were distinguishable from the much thicker, high freeboard MY floes nearby which were not surveyed. In Wilkes land (Fig. S1b) the perennial ice edge was well south of the survey area. Because of the failure of ENVISAT about a month later, it is not possible to determine if significant MY ice drifted into the region.

Most previous reports of MY ice indicate very thick (significantly greater than 2m) for level ice[18,37]. MY ice typically has lower salinity than FY ice[37,38] The structure often shows signs of significant internal melt and refreezing, particularly at the surface where superimposed ice with very low $\delta^{18}O$ values (< -10 , typical of the overlying snow cover) formed by freezing of snow melt water on the ice surface is a tell-tale sign of the ice having survived the summer season[18]. This is often accompanied by icy and very coarse-grained dense snow at the base of the snow pack. The lack of any of these features cannot definitively rule out that a floe is MY ice, but taken together they provide strong evidence that each floe surveyed is most likely to be FY ice.

Ice and snow property data (salinity, crystal structure, and $\delta^{18}O$) for each floe also generally supports the case for FY ice (Table S1, Fig. S2). For the Bellingshausen Sea (Floes 1-5), there was no evidence for superimposed ice based on structure, salinity and $\delta^{18}O$ data in any of the floes, indicating an absence of ice that survived the prior summer. Salinities in the lower portion of the core (excluding surface snow ice) were low, but consistent with warm, thick FY ice that had experienced some drainage. Surface salinities are also consistent with FY ice, although these were affected by flooding and snow ice formation for all cores except for Floe 3. $\delta^{18}O$ values at the surface contrast clearly with a core from a MY floe in the Weddell Sea located near the surveyed floes (Fig S2, red curves). The surface $\delta^{18}O$ of -12.3 ‰ was accompanied by a salinity of < 1 ‰ (not shown), and structure data that showed clear evidence for superimposed ice. The presence of a sunken superimposed ice layer at 100 cm depth shows clearly that the superimposed ice was not formed this season. This contrasts with all other cores that show no buried superimposed ice layer. Where surface $\delta^{18}O$ in the other cores is significantly negative (-5 to -10 ‰), it is accompanied by a high salinity (Table S1) suggestive of snow ice. Snow properties also support FY ice based on a lack of very dense, icy snow (with the possible exception of floe 5), but surface flooding could also obscure this.

For the Weddell Sea floes, ice morphology, structure, and salinities all suggest FY ice. Surface snow and ice melt did lead to a thin (< 20 cm) layer of superimposed ice on each floe (Table S1 and Fig. S2), but the saturated snow cover and ponding on the surface indicate that this most likely formed in the month prior to the survey. For Floes 8-10, all ice property evidence also support FY ice, with salinities typical of FY ice (Table S1). There was no evidence for superimposed ice. One snow pit on floe 7 did have dense icy snow at the base.

This evidence suggests that it is most likely that most or all floes are FY ice. Potential exceptions include Floe 2 based on it's proximity to MY ice in SAR imagery, Floe 5 based on some snow cover characteristics (though SAR imagery strongly suggests against this), and Floe 8, based on limited snow cover characteristics. We cannot definitively rule out that one or more floes, or portions of floes are composed of MY ice. However, this is not crucial to the conclusions of this study. The AUV surveys reveal that all floes were significantly thickened by substantial deformation, whether part of the original floe was composed of MY ice or not.

Multibeam data processing

The Seabed AUV builds a 3-D map of ice draft by integrating ranges measured by the multibeam sonar with vehicle pose estimates within a smoothing and mapping optimization framework[39,40]. The primary sources of navigation information are the fibre optic gyro (for roll, pitch, and heading, measured at 10 Hz), the DVL (for 3-D velocity, measured at 10 Hz), and a Paroscientific digiquartz pressure sensor (for depth, measured at 0.5 Hz). The multibeam measures ranges to the ice at 10 Hz. Because the DVL only works reliably while the AUV is under ice, a small long-baseline acoustic network is deployed from the ship and/or the ice to allow the AUV to move in a floe-relative local reference frame at all times.

A latency value is estimated for each navigation sensor relative to the multibeam by cross-correlating redundant measurements – under level ice, for example, multibeam ranges can be used to estimate vehicle roll, and changes in overall range correlate with changes in vehicle depth. The attitude of the multibeam heading and the roll and pitch biases of the DVL relative to the AUV's navigation frame are also computed as part of the optimization. The AUV survey is designed to provide multibeam sonar overlaps up to 50% trackline to trackline. Overlapping submaps are built under the assumption that local AUV navigation estimates are consistent; these submaps are then aligned with each other, inducing nonlocal constraints on the overall estimate of the AUV's trajectory and binned at 0.5m resolution.

Error associated with AUV-derived sea ice draft

The errors can be broken down into those due to sensor accuracy, fundamental errors in the production of the bathymetric maps, errors in vehicle navigation, and any unresolved errors. For the sensors, the errors are small. The Octans 3000 inertial measurement unit has an error of ~0.1 degrees in pitch and roll, which translates to about 3 cm error in range at 20 m. The Imagenex deltaT 245 kHz multibeam sonar has a range error of <4 cm at that depth. The pressure sensor has an error of < 1 cm. Errors due to sound speed variation will be ~2 cm. The nominal accuracy is then ~5 cm.

The AUV mapping efforts are a continuation of techniques that have been utilized for marine mapping[41,42] in the areas of marine archaeology, marine geology, coral reef ecosystems and naval mine counter measures mapping. This methodology has been validated against optical imagery and photomosaicking techniques[40]. The error in the production of these maps is explored in Figure 12 of REF 40. Here, the error can be computed by examining the variance within individual map bins where there are multiple ranges due to overlapping swaths. The variance is seen here to be of order 1 cm, so this is not a significant source of error.

There is greater error in the horizontal dimensions of the map due to positioning errors relating to navigation. The footprint size of the multibeam at 20m range is ~25 cm. While draft may vary within the footprint and the range may vary depending on the shape of the ice underside within that footprint, the effect is negligible averaged over all ranges on the floe (as demonstrated in Fig. 12 of REF 40). In addition the horizontal position of a given pixel is constrained by the pose estimate of the AUV by the DVL navigation to ~25 cm.

We have therefore binned the data to 50 cm resolution and this only affects the positioning of draft elements.

Unresolved errors (e.g. due to unresolved latency in the sensors) are estimated to be < 10 cm by examining the variation in draft over level ice areas. Relative to the measured mean drafts, this error is small and has no impact on the significance of the results.

Supplementary References

37. Gow A.J., Ackley, S.F., Buck, K.R. & Golden, K. M. Physical and structural characteristics of Weddell Sea pack ice. *CRREL Rep.* 87-14 (1987).

38. Haas, C., Thomas, D, & Bareiss, J. Surface properties and processes of perennial Antarctic sea ice in summer. *J. Glaciol*, **47**, 613–625 (2001)

39. Kaess, M. Ranganathan, A., & Dellaert, F. Incremental Smoothing and Mapping. *IEEE. J. Robotics*. **24**, 1365–1378 (2008).

40. Kunz, C. & Singh, H. Map Building Fusing Acoustic and Visual Information using Autonomous Underwater Vehicles. *J. Field Robotics*, **30**, 763–783 (2013).

41. Singh, H., Whitcomb, L., Yoerger, D. & Pizarro, O. Microbathymetric Mapping from Underwater Vehicles in the Deep Ocean. *J. Comp. Vision*, **79**, 143–161 (2000).

42. Roman, C & H. Singh. Self Consistent Bathymetric Mapping from Robotic Vehicles in the Deep Ocean, *J. Field Robotics*, **24**, 23–50 (2007).

Supp. Figures

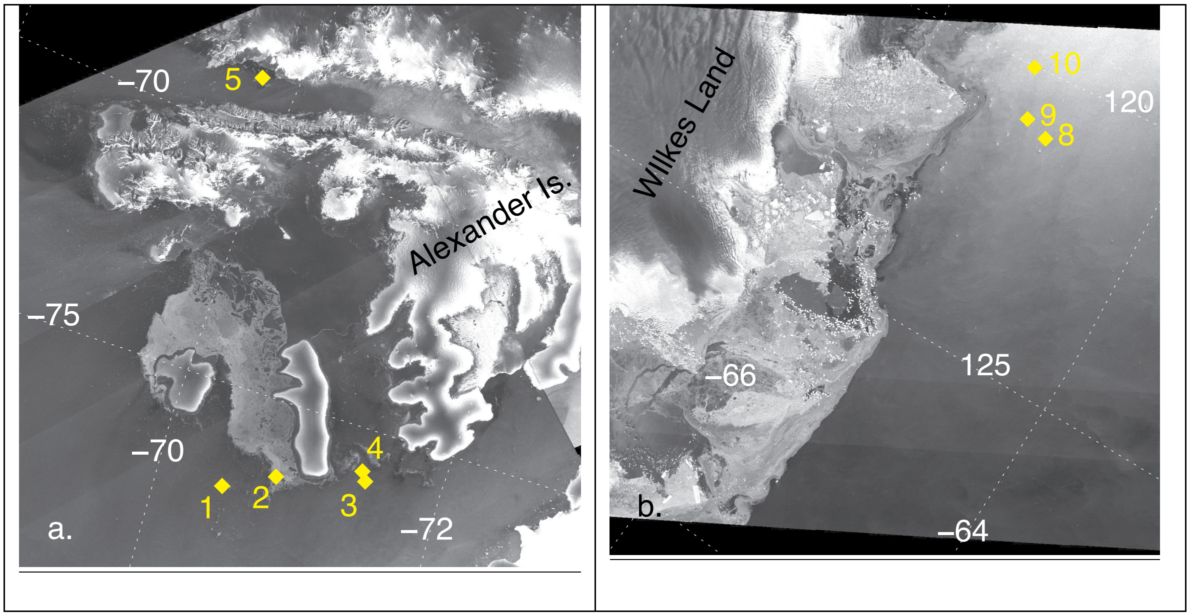

Figure S1

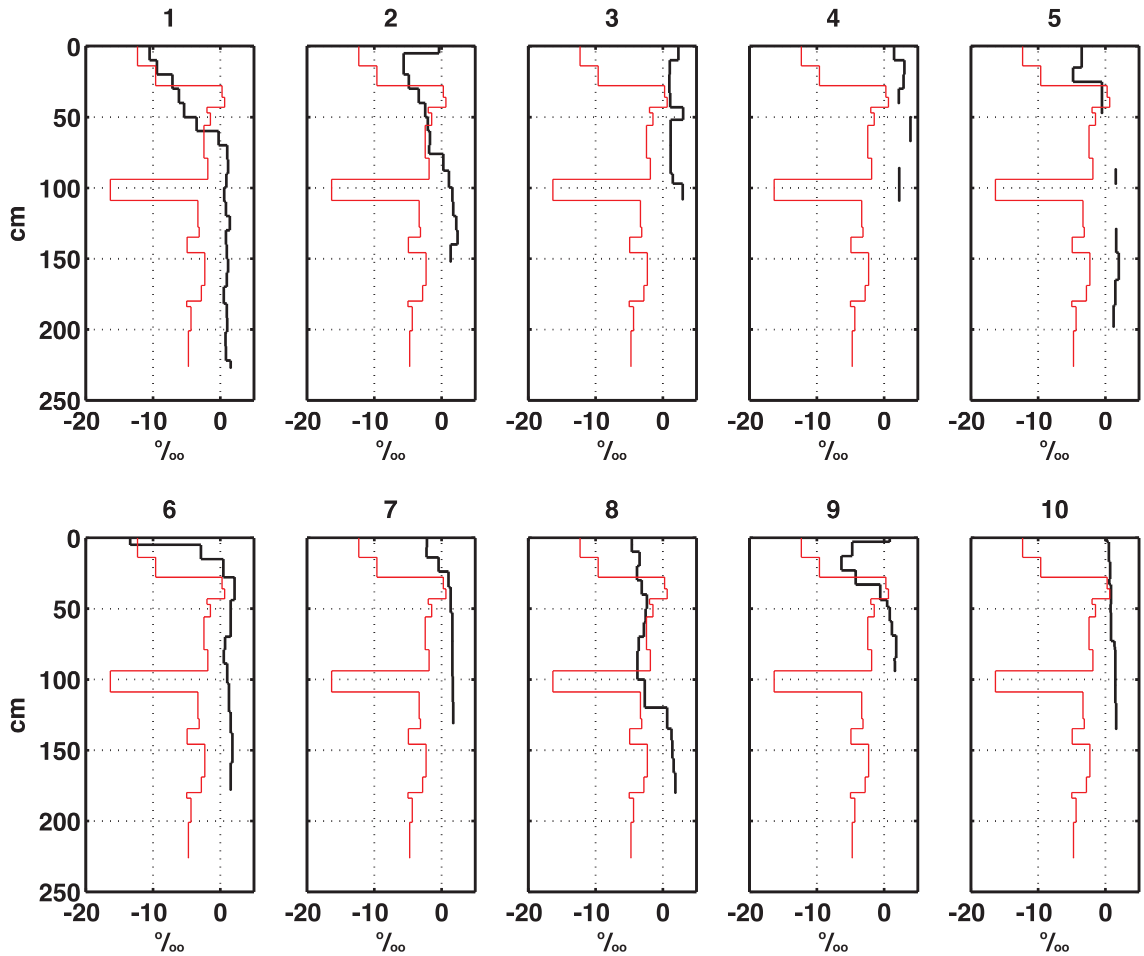

Figure S2

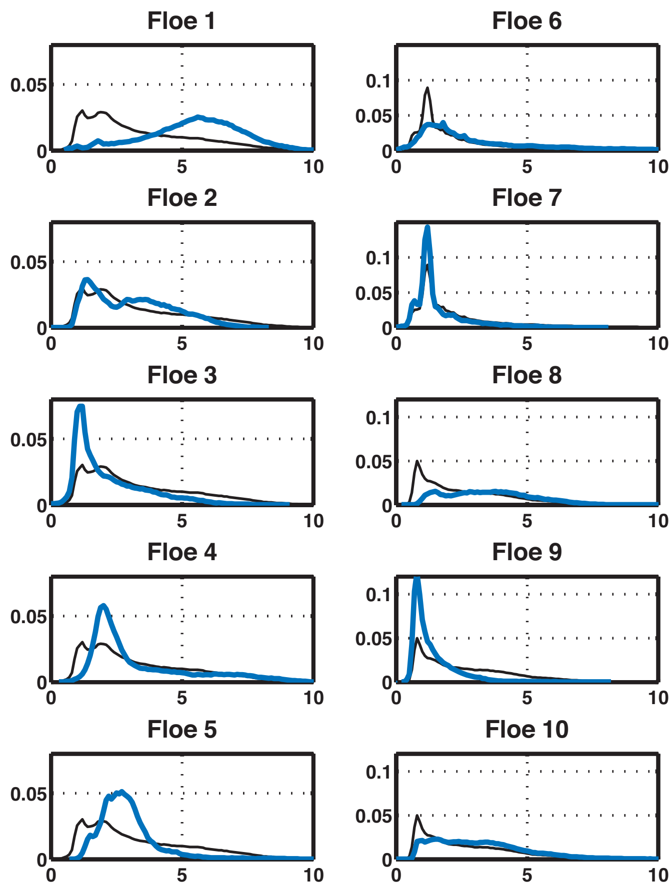
Floe 1
Floe 2
Floe 3
Floe 4
Floe 5
Floe 6
Floe 7
Floe 8
Floe 9
Floe 10
0.05
0.1
0
5
10

Figure S3

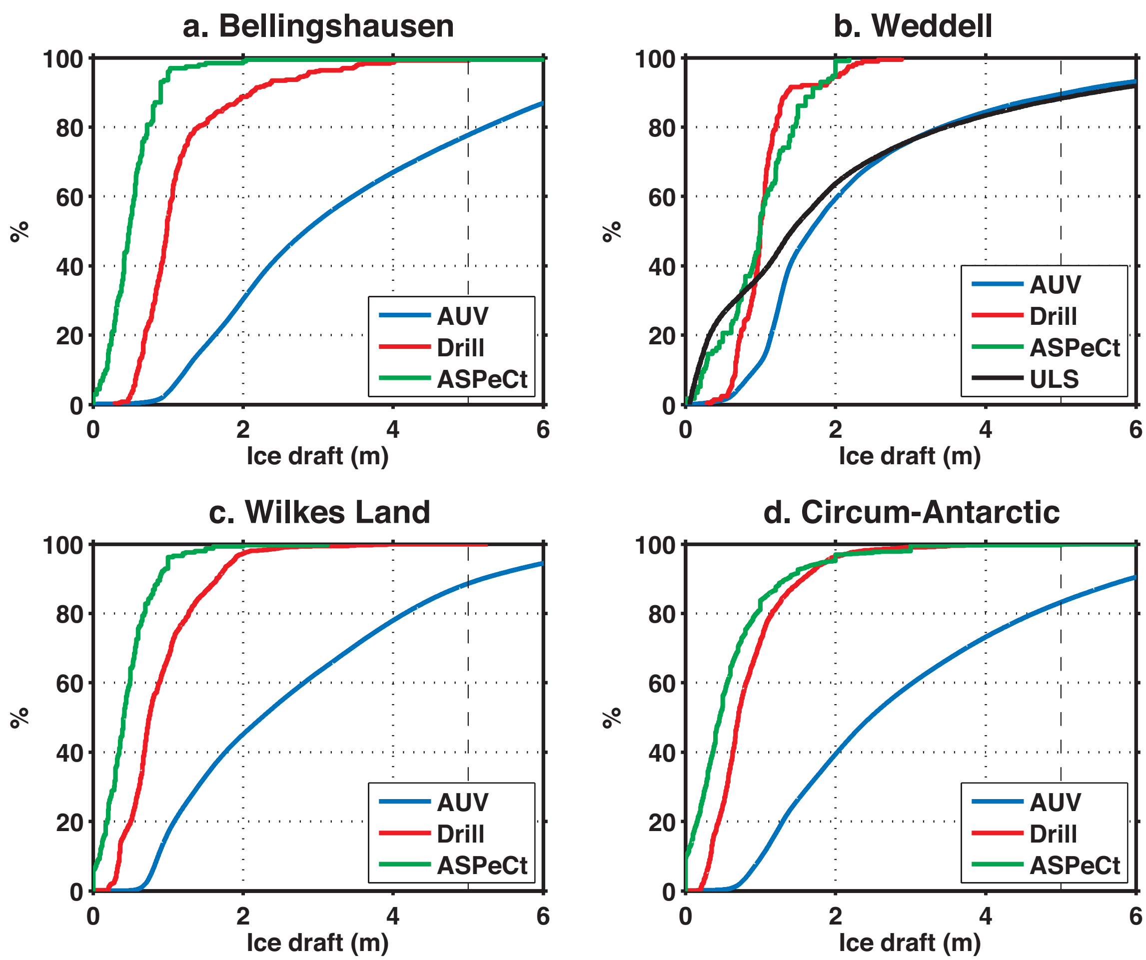

144

145 **Figure S4**

146

Supplementary Figure Captions

Figure S1: ENVISAT Synthetic Aperture Radar imagery showing location of most surveyed floes were in open water the summer prior to the surveys. a Composite of images on Feb 14 and 26, 2010 in the Bellingshausen Sea. Most survey locations were devoid of perennial ice, and unlikely to have such ice drift into the area after freeze-up. **b** Image from March 8, 2012 near Wilkes Land showing retreat of the summer ice cover to the south of the survey locations.

Figure S2: δ^{18}O profiles from ice cores from each floe. Most floes do not have very negative δ^{18}O values (dry snow δ^{18}O ~ -12 to -20‰ during IceBell) at the surface that would indicate superimposed ice on perennial ice. Moderately negative surface δ^{18}O values (0- -10‰) coincide with high salinities (see Table S1) indicative of snow ice. Missing or contaminated values are indicated by breaks in the profile. Red curve: Multiyear floe from the Weddell Sea. The very low (< -10‰) δ^{18}O values at the surface and at 100 cm accompanied by near zero salinity (not shown) indicate superimposed ice.

Figure S3: Normalised histograms of ice draft (m) for individual floes. (**a—j**) Histograms for floes 1—10 from Fig 3 (blue lines) and the sum of all floes specific to each region (black).

Figure S4: Cumulative probability distribution function of AUV and ASPeCt data. Curves show the percentage of ice below a given ice draft (AUV, ULS and Drill) or thickness (ASPeCt), following Fig 3.

Supplementary Tables

Table S1 Evidence for First Year Ice. Ice core and snow data that suggest FY ice (bold) or MY ice (italics). Other entries are ambiguous. Surface salinity is for the top 20 cm, except for Floes 6 and 7 where it is the salinity of the superimposed ice layer. Bottom salinity is either the average salinity of ice below 20 cm, or where $\delta^{18}O > 0$ ‰ to exclude high salinity snow ice layers. **1.** Surface salinity consistent with FY ice but affected by snow ice formation **2.** Superimposed ice present, but likely formed just prior to sampling.

Table S1. IceBell and SIPEX-II floe and ice property characteristics

Floe	**Imagery with ice prior summer?**	**Bottom Salinity (psu)**	**Surface Salinity (psu)**	**Super-imposed Ice/$\delta^{18}O$ (‰)**	**Dense, icy snow at base?**	**Thickness of level pans (m)**
1	**no**	**4.1**	12.1[1]	**no/-10.5**	no (slush)	1.85
2	*ice edge*	**3.7**	4.2[1]	**no/-0.4**	no (slush)	**1.35**
3	**no**	**4.2**	**4.6**	**no/2.4**	**no**	**1.20**
4	**no**	**4.2**	10.4[1]	**no/1.5**	no (slush)	*2.00*
5	**no**	**6.8**	9.7[1]	**no/-3.5**	*yes* (slush)	1.55
6	Mixed drifting Pack	**3.8**	0.4[2]	yes[2]/*-13.3*	yes[2] (saturated)	**1.50**
7	Mixed drifting Pack	**3.3**	4[2]	yes[2]/-2.2	yes[2] (saturated)	**1.20**
8	**no**	**5.3**	7.2[1]	**no/-4.6**	*limited*	**1.50**
9	**no**	**4.8**	**7.1**	**no/0.9**	**no**	**0.80**
10	**no**	**5.4**	**7.6**	**no/0.3**	**no**	1.55

Table S2: Sources of drilling data. Late winter/early spring cruises with ice station drilling data used for comparisons in Fig. 3 and Table 1 from REF 12. Locations of stations are shown in Fig. 1.

Voyage	Date	Sector	Lead Nation
SIPEX – I	2007	Wilkes Land	Australia
SIMBA	2007	Bellingshausen	US
ARISE	2003	Wilkes Land	Australia
ANT104	1992	Queen Maud	German
ANT72	1988	Weddell	German
ANZFLUX 94	1994	Queen Maud	US

Table S3: AUV Survey details

Floe	Date	Latitude	Longitude	Depth (m)	Regime
1	Nov 20 2010	-70.49	-77.12	850	Cont. Shelf
2	Nov 23 2010	-70.84	-76.6	318	Cont. Shelf
3	Nov 26 2010	-71.46	-76.13	553	Cont. Shelf
4	Nov 27 2010	-71.42	-75.93	623	Cont. Shelf
5	Nov 30 2010	-69.74	-68.76	441	Cont. Shelf
6	Nov 15 2010	-65.78	-53.72	1658	Cont. Slope
7	Nov 16 2010	-65.78	-53.72	1658	Cont. Slope
8	3 Oct 2012	-64.95	121.03	2640	Cont. Rise
9	9 Oct 2012	-65.13	120.87	2912	Cont. Rise
10	12 Oct 2012	-65.25	120.02	2528	Cont. Rise